Food Research International 162 (2022) 111945

Contents lists available at ScienceDirect

Food Research International

journal homepage: www.elsevier.com/locate/foodres

Deconstructing extra virgin olive oil through fractionation processes

Laura Bayés-García *, Teresa Calvet

Departament de Mineralogia, Petrologia i Geologia Aplicada, Facultat de Ciències de la Terra, Universitat de Barcelona, Martí i Franquès, s/n, 08028 Barcelona, Spain

ARTICLE INFO

Keywords:
Polymorphism
Crystallization
Fractionation
Triacylglycerol
Lipid
Olive oil
Tocopherol
X-ray diffraction

ABSTRACT

Arbequina monovarietal extra virgin olive oil (EVOO) was fractionated through a multi-step dry fractionation method. Three of the isolated fractions were selected and analyzed: one being liquid at 4 °C, and two being solid at 4 °C, and at 12 °C. Differential scanning calorimetry (DSC) combined with synchrotron radiation X-ray diffraction (SR-XRD) techniques were employed to monitor the polymorphic crystallization and transformation processes when samples were cooled from the melt to complete crystallization and reheated at a rate of 2 °C/min. Fatty acid profiles and α-tocopherol contents were also determined for EVOO and associated fractions. Each sample exhibited a different and unique crystallization and polymorphic behavior, and the number of crystallizing forms and complexity of transitions increased for solid fractions. In more detail, just two polymorphs (β'_3-2L and β'_2-2L) were detected in the liquid fraction, whereas the fraction which remained in the solid state at 12 °C exhibited six different phases (α-2L; β'_3-2L; β'_2-2L; β'_1-2L; β'_2-3L; β'_1-3L). These dissimilarities were strongly correlated with meaningful variations in the fatty acid moieties forming TAG structures and caused large deviations in the crystallization and melting temperatures. As an example, melting temperatures of the liquid and the solid fraction at 12 °C were about −3 °C and 17 °C, respectively. It may be worth exploring the potential of EVOO fractions to be used for improving properties of food stuff, among others. The liquid fraction may be of interest due to its high nutritional value owing to elevated contents in monounsaturated fats and antioxidants, whereas the solid fraction at 12 °C may become a good choice to be used as a high-oleic soft fat.

1. Introduction

Extra virgin olive oil (EVOO), which is obtained by extraction from the olive fruit without the use of any heating treatment or chemicals, becomes one of the highest-value agricultural products due to its unique sensory, health and nutritional properties (Harwood, & Yaqoob, 2002; Cicerale, Lucas, & Keast, 2012). Being typical from the Mediterranean basin, its commerce and increasing demand has been extended worldwide, and its versatility has permitted its usage as flavoring and in multiple formulated food stuff, such as sauces and dressings. Furthermore, its high contents in antioxidants, like tocopherols or phenolic compounds, substantially contribute to its oxidative stability and heat resistance, making it very suitable to be used as cooking oil (Pellegrini, Visioli, Buratti, & Brighenti, 2001; Gutierrez, Arnaud, & Garrido, 2001; Wagner, & Elmadfa, 2000).

Another major contribution to the healthfulness of EVOO is its fatty acid composition, mainly constituted by monounsaturated oleic acid (C18:1). Similarly to other edible lipid systems, fatty acids are primarily present esterified in glycerol structures forming triacylglycerol (TAG) molecules. Thus, oleic acid, together with saturated palmitic (C16:0), stearic (C18:0) and diunsaturated linoleic acid (C18:2), are assembled within different TAG structures mainly forming 1,2,3-trioleoyl glycerol (OOO), 1-palmitoyl-2,3-dioleoyl glycerol (POO), 1-palmitoyl-2-oleoyl-3-linoleoyl glycerol (POL), 1-stearoyl-2,3-dioleoyl glycerol (SOO) and 1,2-dipalmitoyl-3-oleoyl glycerol (PPO) TAG components, among others (Jiménez Márquez, & Beltrán Maza, 2003; Jiménez Márquez, Beltrán Maza, Aguilera Herrera, & Uceda Ojeda, 2007). Relative proportions of these main TAGs may significantly vary depending on the olive variety, the geographical origin or the climate conditions (Vlahov, & Angelo, 1996; Damiani, Cossignani, Simonetti, Campisi, Favretto, & Gabrielli Favretto, 1997; Vichi, Pizzale, & Conte, 2007; Maggio, Barnaba, Cerretani, Paciuli, & Chiavaro, 2014).

Regardless of the low melting temperature of EVOO, the study of its crystallization and polymorphic behavior becomes interesting and fundamental for application at chilled temperatures, but also for food authentication (Ferrari, Angiuli, Tombari, Righetti, Matteoli, & Salvetti, 2007; Bayés-García, Tres, Vichi, Calvet, Cuevas-Diarte, Codony, Boatella, Caixach, Ueno, & Guardiola, 2016; Bayés-García, Colomer-

* Corresponding author.
E-mail address: laurabayes@ub.edu (L. Bayés-García).

https://doi.org/10.1016/j.foodres.2022.111945
Received 14 June 2022; Received in revised form 21 July 2022; Accepted 12 September 2022
Available online 17 September 2022

Llombart, Aguilar-Jiménez, & Calvet, 2021), the determination of fraudulent practices (Chiavaro, Vittadini, Rodriguez-Estrada, Cerretani, Capelli, & Bendini, 2009), and even for fractionation processes (Timms, 2005; Zaliha, Chong, Cheow, Norizzah, & Kellens, 2004; Kellens, Gibon, Hendrix, & De Greyt, 2007; Chaleepa, Szepes, & Ulrich, 2010; Bootello, Garcés, Martínez-Force, & Salas, 2011), as we will analyze in the present work. Among the existing fractionation methodologies, dry fractionation is, despite its lower efficiency, the least contaminant one and does not require the use of additives, as it is simply based on the crystallization behavior of the fat.

Crystallization characteristics and polymorphism of lipids are determinant in resulting physicochemical properties, including melting behavior, and textural and rheological properties (Larsson, Quinn, Sato, & Tiberg, 2006). Our group systematically characterized the complex polymorphism of main pure TAGs present in EVOO (Bayés-García, Calvet, Cuevas-Diarte, Ueno, & Sato, 2013; Bayés-García, Calvet, Cuevas-Diarte, & Ueno, 2016) and, as a step forward, the crystallization behavior of EVOO through the mixtures of TAG components, from binary and ternary to multi-component systems (Bayés-García, Calvet, Cuevas-Diarte, & Ueno, 2017). The selected EVOO under study was an Arbequina monovarietal type, and the results were interpreted by considering three main groups of previously-studied TAGs having different molecular structures: triunsaturated OOO and OOL, saturated–unsaturated-unsaturated POO, POL and SOO, and saturated-saturated–unsaturated PPO. As expected, TAGs belonging to the same structural group displayed a highly similar polymorphic behavior, and the polymorphism of EVOO was equivalent to that of the 6 TAG elements mixture, so that minor components did not play a determining role.

In the present work, we analyzed the polymorphic crystallization and transformation of an EVOO obtained from the same olive variety (being 100 % Arbequina), as variations in the nature of olive may result in differences in the behavior exhibited by the samples. Then, instead of simulating an EVOO through multi-component mixtures, as in previous work (Bayés-García, Calvet, Cuevas-Diarte, & Ueno, 2017), we made the opposite, we deconstructed it through fractionation processes. We are sure that previous knowledge acquired permitted an accurate interpretation of the data obtained.

A first attempt in fractionating EVOO was carried out by Jansen & Birch (2009). Authors performed a one-step process to obtain two different fractions: one being liquid at 4 °C and one solid at the same temperature. They determined the melting profiles, fatty acid and antioxidant compositions, and heating resistance of the fractions obtained, and concluded that it is possible to fractionate EVOO without compromising stability towards oxidation. In the present work, we carried out a multi-step fractionation process by successively increasing the crystallization temperature, and characterized three of the fractions obtained: one being liquid at 4 °C, one solid at the same temperature, and one being solid at 12 °C. The crystallization and polymorphic conduct was studied by differential scanning calorimetry (DSC) and synchrotron radiation X-ray diffraction (SR-XRD) when samples were subjected to a thermal treatment based on cooling from the molten state to complete crystallization and reheated at a rate of 2 °C/min, and compared to that of EVOO under the same experimental conditions. To the best of our knowledge this is the first work in which the polymorphic crystallization of associated fractions of EVOO is analyzed. Furthermore, the polymorphic differences observed between samples were interpreted by considering variations in TAG compositions of EVOO fractions. Fatty acid profiles and tocopherol contents were also determined for the samples under study.

It may be highly interesting to explore the multiple possibilities of EVOO fractions for application in food stuff and others. More liquid fractions may be considered due to its high nutritional value attributable to high contents in unsaturated fats and antioxidants, whereas solid fractions may be also of special interest for the development of soft fats. The usage of oleic-rich semi-solid fats may become a compelling approach in the reduction of saturated fats and the formulation of trans fatty acids alternatives.

2. Materials and methods

2.1. Materials

The EVOO sample (100 % Arbequina variety, Les Garrigues, Spain) was donated by Gralisa Oils S.A. (Cabrera de Mar, Spain).

2.2. EVOO fractionation

The fractionation procedure employed was based on that described by Jansen & Birch (2009), but with some modifications and additional steps at varied temperatures. 70 ml of the EVOO sample were incubated at 4 °C for 7 days and then centrifuged by using a Mikro 220R apparatus (Hettich, Tuttlingen, Germany). Centrifugation was carried out at the same temperature at 3000 rpm for 30 s to force the separation of the liquid and solid phases. The liquid fraction obtained (named *Liquid 4 °C* from now on) was extracted, the solid phase melted and the full process repeated three times more in order to improve the separation process. The liquid entrapped in the solid fraction was removed by absorption by filter paper in a cold room at 6 °C. An aliquot of the resulting phase (named *Solid 4 °C* from now on) was taken for analyses and the rest was melted and subjected to further fractionation processes. These consisted of progressively increasing the incubation and centrifugation temperature until no crystallization occurred. Then, the highest temperature at which crystallization still occurred within the predetermined amount of time was 12 °C. The liquid entrapped in the solid fraction obtained at such conditions (named *Solid 12* °C from now on) was also removed by following the methodology previously described.

2.3. Differential scanning calorimetry

DSC experiments were carried out at atmospheric pressure by using a PerkinElmer DSC-8000 apparatus (Perkin Elmer, Waltham, MA, USA). Samples (8.000–8.500 mg) were weighed into 50 μl aluminum pans and an empty pan was used as reference. The instrument was calibrated with reference to the melting temperatures and enthalpies of indium and decane standards. Dry nitrogen was used as purge gas in the DSC measurement chamber at a flow rate of 20 cm^3/min. Thermograms were analyzed using Pyris software to obtain T_{top} and T_{onset} (or T_{end}) transition temperatures. T_{top} corresponded to the temperature at peak-top positions, whereas T_{onset} (or T_{end}) was defined as the temperature at intersections between baselines and tangents at inflection points of the initial (or final) peak slopes.

During measurements, samples were cooled from 45 °C, temperature at which they were completely molten, to −80 °C and subsequently heated at a constant rate of 2 °C/min. Three independent measurements were conducted for all samples and the results were evaluated for random uncertainty with a 95 % threshold of reliability using the Student's method.

For further interpretation of DSC thermograms, SR-XRD experiments were carried out under the same selected thermal treatment.

2.4. Synchrotron radiation X-ray diffraction

Synchrotron radiation X-ray diffraction (SR-XRD) experiments were conducted on beamline BL11-NCD-SWEET at the synchrotron ALBA (Cerdanyola del Vallès, Barcelona, Spain) at 12.4 keV. The sample-detector distance was 2.7 m. X-ray scattering data were collected on a Pilatus 1 M detector with a pixel size of 172 μm × 172 μm for the small-angle X-ray diffraction (SAXD) data, and on a LX255-HS Rayonix detector with a pixel size of 88 mm × 88 μm for the wide-angle X-ray diffraction (WAXD) data. The temperature of the sample was controlled by a Linkam stage. The q-axis calibration was obtained by measuring silver behenate for SAXD and Cr_2O_3 for WAXD. The program pyFAI was

used to integrate the 2D SAXD and 2D WAXD into the 1D data.

2.5. Fatty acid composition

Fatty acids compositions of EVOO and associated fractions were determined by gas chromatography at the Scientific and Technological Centers (CCiTUB) of the Universitat de Barcelona. Samples were extracted through transterification with potassium hydroxide in methanol at room temperature. Briefly, 20 mg of each sample were placed in a centrifuge tube and dissolved in 2 ml heptane, and a volume of 200 μl of 2 M potassium hydroxide in methanol solution was added to each sample. After vigorously mixing the tube, the heptane layer was transferred to a vial when clear. Samples were processed by duplicate, and a duplicate of blank sample was processed in parallel. A calibration curve of fatty acid methyl esters was used for quantitation.

The equipment consisted of a Shimadzu QP2010 (Kyoto, Japan) coupled to a SGE BPX70 column (30 m _ 0.25 mm, 0.25 μm). The injector temperature was 260 °C, and the injection mode was splitless, with a splitless time of 1 min. Helium was the carrier gas, with a gas flow of 1.00 ml/min, and oven temperature was programmed from 60 °C (1 min) to 260 °C (1 min) at a rate of 15 °C/min. Transfer line and ion source temperatures were set at 260 °C. Mass spectra were obtained in the electron ionization mode at 70 eV. Acquisition mass range was from 50.00 to 550.00 amu with a solvent delay of 2.70 min.

2.6. Tocopherol analysis

Tocopherol content was also determined at the Scientific and Technological Centers (CCiTUB) of the Universitat de Barcelona by high-performance liquid chromatography (HPLC), using α-tocopherol as external standard. Oil samples were dissolved in hexane and analyzed on a system consisting of a Kromasil 100Si 5 μm 15x0.46 cm column (Teknokroma, Sant Cugat del Vallès, Spain), an FP-1520 fluorescence detector (Jasco, Hachioji, Tokyo, Japan), and a 600 controller pump and a 717plus injector (both by Waters, Milford, MA, USA). Hexane/dioxane (95.5/4.5 v/v) was used as mobile phase, and the flow rate was 1.0 ml/min.

3. Results and discussion

3.1. Crystallization and polymorphic behavior of EVOO and associated fractions

The EVOO sample and associated fractions (Liquid 4 °C, Solid 4 °C and Solid 12 °C) were subjected to the same dynamic thermal treatment consisting of cooling from the melt (45 °C) to −80 °C at 2 °C/min and heated thereafter at the same constant rate (see corresponding DSC curves in Fig. 1). For clarity, long- and short-spacing values (nm), which

Table 1
Long-spacing (LS) and short-spacing (SS) values of EVOO sample and its fractions.

	LS (nm)	SS (nm)
β'$_3$-2L	5.4; 2.7	0.42; 0.38
α-2L	4.8	0.42
β'$_2$-2L	4.4	0.45; 0.43; 0.39
β'$_2$-3L	6.2–6.3	0.45; 0.43; 0.39
β'$_1$-3L	6.4; 3.2	0.45; 0.43; 0.39
β'$_1$-2L	4.2	0.43; 0.39

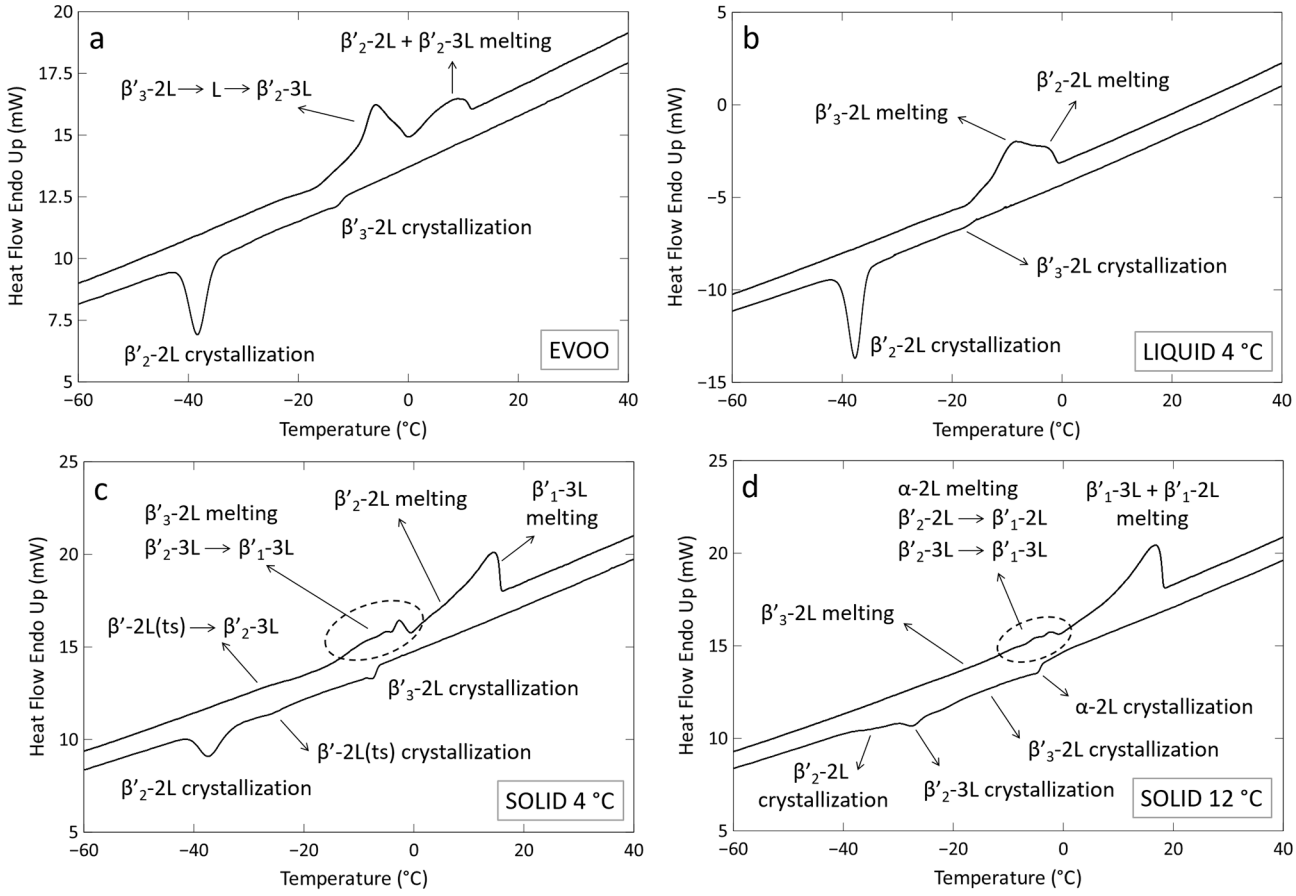

Fig. 1. DSC thermograms acquired when samples were cooled from 45 °C to −80 °C and reheated both at 2 °C/min. a) EVOO (100 % Arbequina variety); b) Liquid 4 °C fraction; c) Solid 4 °C fraction; d) Solid 12 °C fraction.

permitted the identification of each polymorphic form of EVOO and its fractions, are presented in Table 1. A total of six different polymorphic forms, mainly β' forms with either double (2L) or triple (3L) chain-length structure, were detected. However, most of the samples did not exhibit the occurrence of all polymorphs. In general, the complexity of crystallization and transformation processes increased as the melting temperature of the sample was higher, that is for solid fractions at 4 and 12 °C, as will be described further on.

Fig. 1a and 2 show the thermal behavior and corresponding SR-XRD patterns (SR-SAXD and SR-WAXD simultaneous measurements), respectively, for the EVOO sample. Moreover, most representative DSC transition temperatures are shown in Table 2. When EVOO was cooled, and exothermic signal, with T_{onset} of −11.7 °C and T_{top} of −13.4 °C, was observed and it was assigned to the crystallization of β'$_3$-2L form (occurrence of SR-SAXD peaks at 5.5 and 2.8 nm, and SR-WAXD signals at 0.42 and 0.37 nm). On further cooling, additional reflections at 4.4 nm (SR-SAXD), and 0.45, 0.43 and 0.39 nm (SR-WAXD) were observed at around −44 °C and attributed to the β'$_2$-2L form crystallization. This phenomenon corresponded to the DSC exothermic signal with onset and peak temperatures of −35.5 °C and −38.4 °C, respectively (see Fig. 1a and Table 2). When the fully crystallized sample was afterward heated, melt-mediated transformation occurred from β'$_3$-2L to a new β'$_2$-3L form, as according to the SR-XRD data, the β'$_3$-2L polymorph melted at around −8 °C (disappearance of peaks at 5.5 and 2.8 nm, and at 0.42 and 0.37 nm) and, soon after, β'$_2$-3L was formed (rise of SR-SAXD peak at 6.3 nm, see enlarged image in Fig. 2a). These events were associated to the first broad endothermic DSC signal with onset and peak temperatures of −10.5 °C and −6.3 °C, respectively. Then, at about 0 °C, β'$_2$-2L, followed by β'$_2$-3L at 10 °C, melted. These successive melting processes were easily distinguished through the vanishing of characteristic SR-SAXD peaks and matched with the single broad endothermic event with onset, peak and end temperatures of 0.8, 7.6 and 11.0 °C, respectively (see Table 2). These results are in agreement with those reported by previous work carried out by our group (Bayés-García, Calvet, Cuevas-Diarte, & Ueno, 2017), although for simplicity we slightly modified the nomenclature of the phases (that is the numbering of β' forms) after considering all the occurring polymorphs in the EVOO fractions obtained.

The crystallization behavior exhibited by the EVOO fraction which still remained in the liquid state at 4 °C (named Liquid 4 °C fraction) became simpler than that of EVOO and most of events occurred at significantly lower temperatures (see Fig. 1b, Fig. 3 and Table 2). According to the DSC data, the crystallization process was initiated at −15.7 °C (T_{onset}) with the occurrence of β'$_3$-2L form (SR-XRD peaks at 5.7 and 2.9 nm, and at 0.42 and 0.37 nm) and it was set 4 °C below compared to the same phenomenon in EVOO. Upon further cooling, additional reflections at 4.4 nm (SR-SAXD) and 0.45, 0.43 and 0.39 nm (SR-WAXD), caused by the β'$_2$-2L crystallization, were discerned and linked to the main exothermic phenomenon with onset, peak and end temperatures of −35.5 °C, −37.6 °C and −40.0 °C. Hence, β'$_2$-2L crystallized at equivalent temperatures in the Liquid 4 °C fraction and EVOO, so that differences during cooling were mainly perceived at the initial temperature of the crystallization process of the samples. Regarding the phase transitions occurring during the subsequent heating step, SR-XRD data revealed the β'$_3$-2L melting at about −13 °C, which was succeeded by that of the β'$_2$-2L polymorph at −1 °C. These phenomena were interpreted through the vanishing of characteristic SR-XRD peaks and assigned to the broad double endothermic DSC event with T_{onset} of −14.6 °C and T_{end} of −0.5 °C. Thus, one may note the noticeable decrease in melting temperatures (around 10 °C in the end melting temperature, see Table 2) compared to the EVOO case. This fact may be in part due to the absence of the β'$_2$-3L polymorph in the Liquid 4 °C fraction, which manifested in EVOO during heating through melt-mediated transformation from β'$_3$-2L and exhibited higher melting temperature than β'$_3$-2L and β'$_2$-2L forms.

As previously stated, the attained solid fractions displayed more complicated crystallization and polymorphic behavior as described below. Regarding the fraction which was in the solid state at 4 °C (named Solid 4 °C), Fig. 1c shows corresponding cooling and heating DSC curves when the sample was subjected to the conditions previously described, whereas associated SR-XRD patterns are presented in Fig. 4. Additionally, most representative crystallization, phase-transition and melting temperatures are summarized in Table 3. When the Solid 4 °C fraction was cooled at 2 °C/min from the molten state, characteristic β'$_3$-2L SR-SAXD peaks at 5.4 and 2.7 nm and SR-WAXD ones at 0.42 and 0.38 nm appeared at about −12 °C. This crystallization process correlated with the DSC exothermic signal starting at −6.6 °C (T_{onset}) and having a peak temperature of −7.7 °C (see Fig. 1c and Table 3). Thereafter, additional SR-SAXD reflections at 5.6 and 2.8 nm, which appeared as a splitting of those already present, were discerned at about –30 °C. This newly-formed β' form, having a double-chain length structure and which expired in short time as we will following describe, was tentatively called β'-2L transient form, that is β'-2L(ts), and its occurrence fitted with the broad and flat exothermic DSC appearing at −26.2 °C (T_{peak}). Later, additional more intense exothermic event commencing at –32.8 °C agreed with the crystallization of β'$_2$-2L (characteristic new diffraction peaks at 0.45 and 0.43 nm). Intricate phase transformation processes occurred during the heating step, based on multiple transitions between very similar polymorphic forms (all being β'), so that SR-SAXD information became highly useful for identification. When heated, new SR-SAXD peak at 6.2 nm (3L) occurred and increased in intensity at the expense of those at 5.6 and 2.8 nm (corresponding to β'-2L(tr) form). In addition, new reflection at 0.39 nm came up and those existing at 0.45 and 0.43 nm were intensified. This leaded us to conclude that β'-2L (ts) may have transformed into β'$_2$-3L and, according to the DSC data, this happened at −27.4 °C (T_{peak}). Following endothermic phenomena detected corresponded to the melting of the firstly crystallized β'$_3$-2L form (vanishing of congruent reflections at 5.4 and 2.7 nm, and those at 0.42 and 0.38 nm at −8 °C) and to a β'$_2$-3L → β'$_1$-3L transformation, which was detected through the shifting of the 3L SR-SAXD peak from 6.2 to 6.4 nm and the occurrence of a new one at 3.2 nm at about −4 °C These events were matched to the broad complex endothermic DSC signal with onset and end temperatures of −14.8 °C and −1.1 °C, respectively (see Fig. 1c). Finally, characteristic diffraction reflections of the already existing β'$_2$-2L and β'$_1$-3L polymorphs respectively vanished at about 4 °C and 16 °C, due to their melting (last endothermic DSC peak beginning at 0.1 °C and with top temperature of

Table 2
Crystallization (c), melting (m) and polymorphic transformation temperatures (°C) of EVOO sample and liquid fraction at 4 °C when cooled from the melt and subsequently heated.

EVOO				
		COOLING		
β'$_3$-2L (c)		β'$_2$-2L (c)		
T_{onset}	T_{top}	T_{onset}	T_{top}	T_{end}
−11.7 ± 0.9	−13.4 ± 1.2	−35.5 ± 1.0	−38.4 ± 0.6	−41.6 ± 0.5
		HEATING		
β'$_3$-2L → L → β'$_2$-3L		β'$_2$-2L + β'$_2$-3L (m)		
T_{onset}	T_{top}	T_{onset}	T_{top}	T_{end}
−10.5 ± 0.4	−6.3 ± 1.1	0.8 ± 0.8	7.6 ± 1.0	11.0 ± 1.0
LIQUID 4 °C				
		COOLING		
β'$_3$-2L (c)		β'$_2$-2L (c)		
T_{onset}	T_{top}	T_{onset}	T_{top}	T_{end}
−15.7 ± 1.1	−18.2 ± 1.7	−35.5 ± 0.6	−37.6 ± 1.0	−40.0 ± 1.1
		HEATING		
β'$_3$-2L (m)		β'$_2$-2L (m)		
T_{onset}	T_{top}		T_{top}	T_{end}
−14.6 ± 0.5	−8.5 ± 0.7		−2.7 ± 0.6	−0.5 ± 1.0

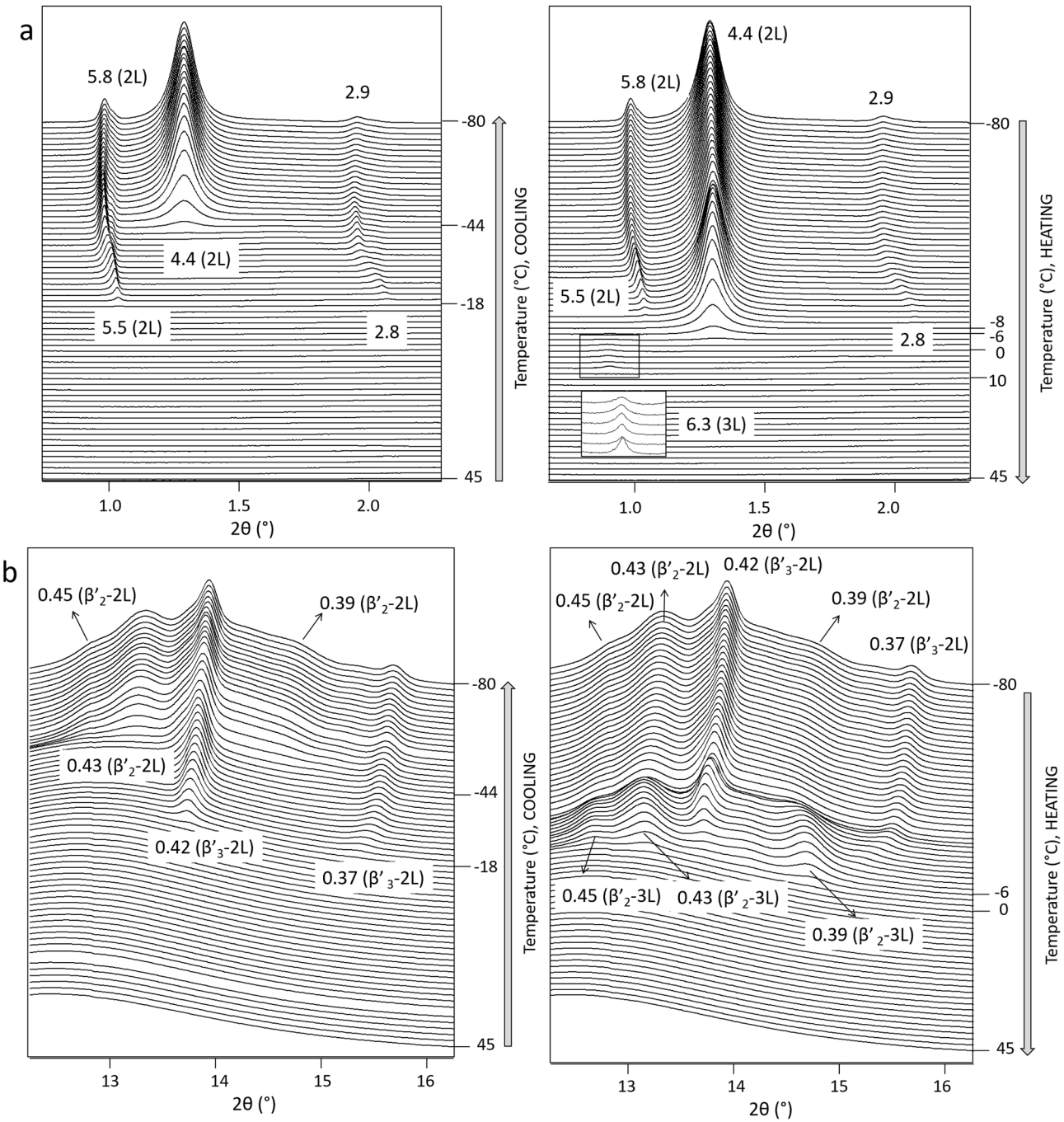

Fig. 2. SR-XRD results of EVOO (100 % Arbequina variety) taken under cooling and subsequently heating both at a rate of 2 °C/min. (a) SR-SAXD and, (b) SR-WAXD patterns. Unit: nm.

13.9 °C).

The EVOO fraction which remained in the solid state at 12 °C (named Solid 12 °C fraction) was subjected to the same thermal procedure. This sample also exhibited a remarkably sophisticated crystallization and transformation behavior and the temperatures at which events occurred became even higher than for the Solid 4 °C fraction. In more detail, when cooled, SR-XRD peaks attributable to an α-2L form (4.8 nm and 0.42 nm) occurred at about −4 °C and it corresponded to the crystallization DSC peak at −3.3 °C (T_{onset}) (see Fig. 1d and 5, and Table 3). One may note that this onset crystallization temperature became 3 °C, 8 °C and 12 °C higher than that of the Solid 4 °C fraction, EVOO sample and the Liquid 4 °C fraction, respectively, and it was in part caused by the presence of this newly-formed α-2L form, which did not take place in other samples.

Around 6 °C below, β'$_3$-2L crystallized (reflections at 5.5 and 2.7 nm, and 0.38 nm), and no specific DSC peak could be solely attributed to this crystallization, so that it may be overlapped with that of the preceding α-2L form. When proceeding with the cooling process, the occurrence of a SR-SAXD peak at 6.2 nm revealed the crystallization of β'$_2$-3L (onset temperature of −25.1 °C, Table 3) and, further on, β'$_2$-2L was detected through typical peaks at 4.4 nm and 0.45, 0.43 and 0.39 nm (Fig. 5) and it was associated to the crystallization peak with top temperature of –33.5 °C. Concerning the phase transformations monitored during heating, SR-SAXD data disclosed the melting of β'$_3$-2L at first through the fading of 5.5 and 2.7 nm peaks. According to the X-ray diffraction data, this event occurred at about −10 °C, although no defined DSC signal was detected around this temperature (Fig. 1d). About 10 °C

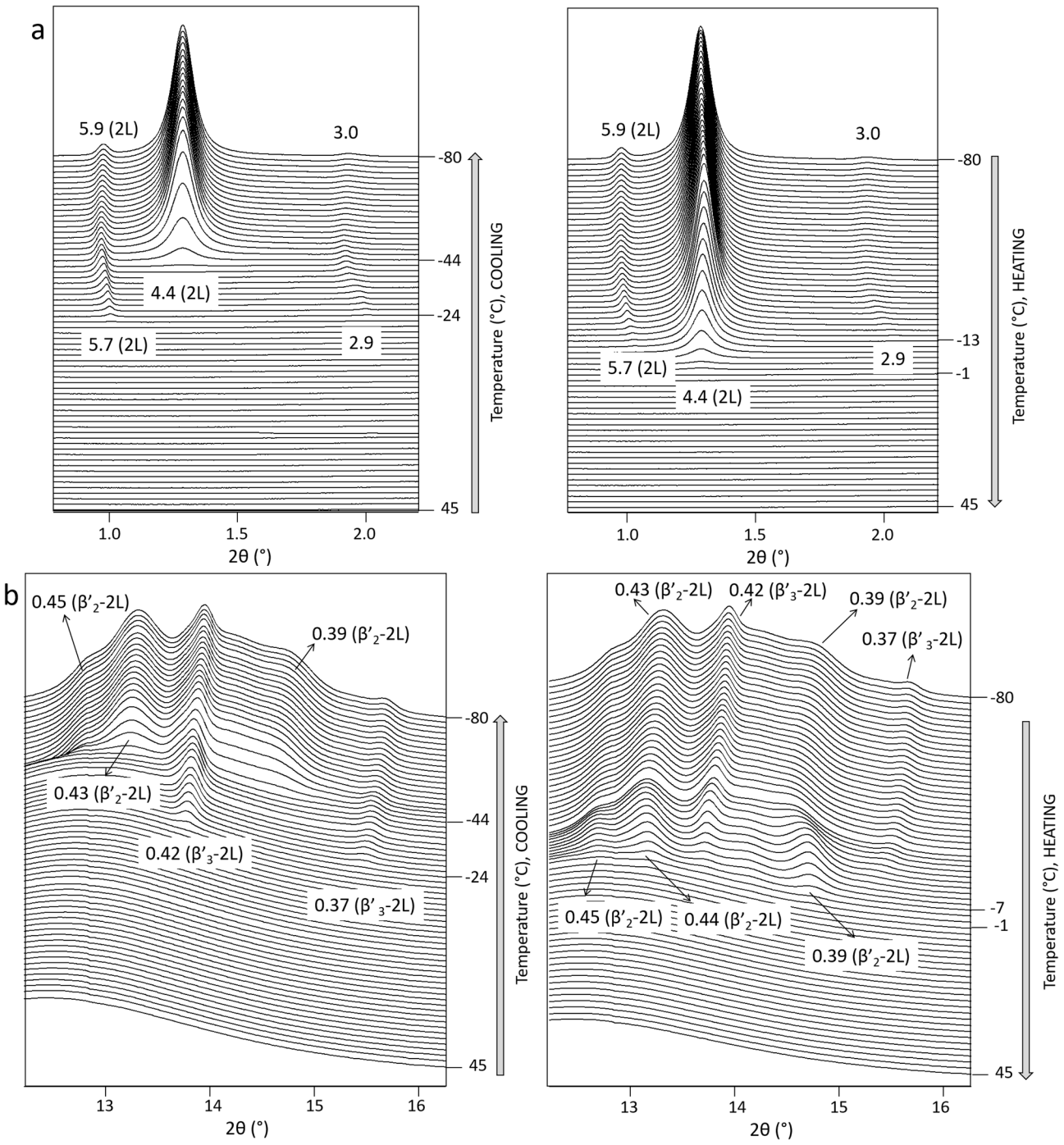

Fig. 3. SR-XRD results of the Liquid 4 °C fraction taken under cooling and subsequently heating both at a rate of 2 °C/min. (a) SR-SAXD and, (b) SR-WAXD patterns. Unit: nm.

forward, that is at a temperature of 0 °C, several simultaneous phenomena in SR-SAXD patterns took place: the reflection at 4.8 nm vanished and that at 4.4 nm shifted to 4.2 nm, while the 3L peak at 6.2 nm displaced to 6.4 nm. Meanwhile, correlated SR-WAXD reflections with d-spacing values of 0.42 and 0.37 nm vanished. These changes were interpreted as the melting of the initially crystallized α-2L form (4.8 nm), and β'_2-2L → β'_1-2L (4.4 → 4.2 nm) and β'_2-3L → β'_1-3L (6.2 → 6.4 nm) polymorphic transformations. This series of episodes were linked to the sophisticated and broad endothermic signal starting at −13.4 °C (T_{onset}) and ending at −1.2 °C (T_{end}) (see Table 3). Finally, the most stable polymorphs attained during this heating process, β'_1-3L and β'_1-2L, melted at about 16.4 °C (T_{top}) and no diffraction peaks were present at 18 °C.

According to the previous results, the four samples analyzed (EVOO, Liquid 4 °C, Solid 4 °C and Solid 12 °C fractions) exhibited a different and unique crystallization and polymorphic behavior, and the number of crystallizing forms and complexity of transitions increased as the melting temperature of the sample increased. Then, EVOO and the Liquid 4 °C fraction displayed much simple polymorphic conduct than the two solid fractions.

Fig. 6 schematically summarizes the crystallization and transformation processes identified for the four analyzed samples when subjected to the same thermal program. Rough temperatures at which phenomena occurred are also indicated. One may easily notice that

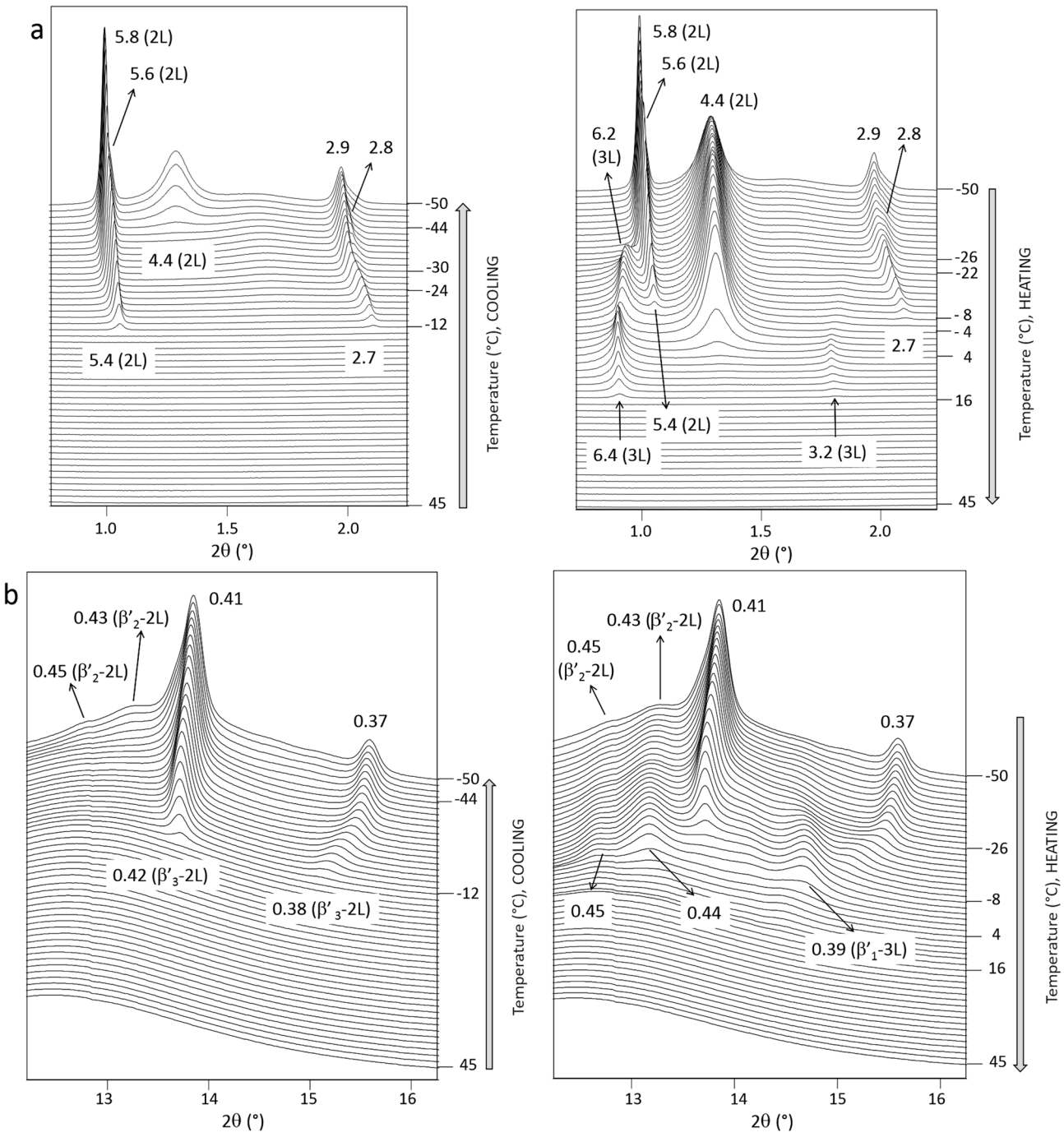

Fig. 4. SR-XRD results of the Solid 4 °C fraction taken under cooling and subsequently heating both at a rate of 2 °C/min. (a) SR-SAXD and, (b) SR-WAXD patterns. Unit: nm.

crystallization and melting occurred at significantly lower temperatures (almost 10 °C) in EVOO than in solid fractions, and temperatures were even lower for the Liquid 4 °C fraction, reaching the highest difference of about 13 °C with the Solid 12 °C fraction. The same occurred with melting temperatures, as EVOO and the Liquid 4 °C fraction showed an end of melting temperature of 11 °C and −0.5 °C, respectively, whereas melting finished at 15.5 °C in the Solid 4 °C fraction, and at 18.1 °C in the Solid 12 °C fraction. This differences are clearly shown in Tables 2 and 3.

EVOO exhibited just three different polymorphs: first crystallizing β'$_3$-2L, β'$_2$-2L, and triple-chain length structure β'$_2$-3L form, which was obtained through polymorphic transformation during the heating step. The behavior displayed by the Liquid 4 °C fraction became very similar, except for the lower temperatures at which events happened, and the non-occurrence of β'$_2$-3L form. The end of melting temperature of EVOO was increased (about 11 °C) with respect to the Liquid 4 °C fraction in part due to the occurrence of this β'$_2$-3L form, which was not detected in the liquid fraction. However, β'$_2$-2L form crystallized at the same temperature in both samples (35.5 °C, see Table 2). This β'$_2$-2L polymorph, having d-spacing values of 4.4 nm and 0.45, 0.43 and 0.39 nm, was the most abundant one in the two samples, as one may figure out by considering the intensity and integrated area of its corresponding DSC crystallization peak (see Fig. 1a and 1b) and that of characteristic SR-SAXD peak at 4.4 nm (Figs. 2 and 3). This polymorphic form may

Table 3
Crystallization (c), melting (m) and polymorphic transformation temperatures (°C) of solid fractions at 4 and 12 °C when cooled from the melt and subsequently heated.

SOLID 4 °C						
			COOLING			
β'$_3$-2L (c)		β'-2L (ts) (c)			β'$_2$-2L (c)		
T_{onset}	T_{top}	T_{top}			T_{onset}	T_{top}	T_{end}
−6.6 ±0.6	−7.7 ±0.6	−26.2 ±1.1			−32.8 ±0.5	−37.2 ±0.8	−40.9 ±0.9
			HEATING			
β'-2L(ts) → β'$_2$-3L	β'$_3$-2L (m) β'$_2$-3L → β'$_1$-3L		β'$_2$-2L + β'$_1$-3L (m)			
T_{top}	T_{onset}	T_{end}	T_{onset}	T_{top}	T_{end}	
−27.4 ±1.5	−14.8 ±1.4	−1.1 ±1.0	0.1 ±0.3	13.9 ±1.3	15.5 ±0.9	
SOLID 12 °C						
			COOLING			
α-2L + β'$_3$-2L (c)			β'$_2$-3L (c)		β'$_2$-2L (c)	
T_{onset}	T_{top}		T_{onset}	T_{top}	T_{top}	T_{end}
−3.3 ±1.0	−5.1 ±0.9		−25.1 ±1.3	−27.4 ±0.7	−33.5 ±1.6	−39.1 ±0.9
			HEATING			
	α-2L (m) β'$_2$-2L → β'$_1$-2L β'$_2$-3L → β'$_1$-3L		β'$_1$-3L + β'$_1$-2L (m)			
	T_{onset}	T_{end}	T_{onset}	T_{top}	T_{end}	
	−13.4 ±1.2	−1.2 ±1.1	4.5 ±0.6	16.4 ±1.2	18.1 ±1.1	

correspond to β' forms of the main TAG of olive oil, OOO, but also of the other main triunsaturated TAG OOL, all the polymorphic forms of which have the same long-spacing value of 4.4–4.5 nm (Bayés-García, Calvet, Cuevas-Diarte, Ueno, & Sato, 2013). Nevertheless, the intensity and integrated area of the same β'$_2$-2L crystallization DSC signal and SR-SAXD peak at 4.4 nm, which was attributed to the triunsaturated OOO and OOL, meaningfully decreased in solid fractions, especially in the Solid 12 °C fraction, as we will describe further on.

As stated, solid fractions exhibited more sophisticated behavior, with a higher number of occurring polymorphs and subsequent phase transitions. Specifically, the Solid 4 °C fraction exhibited four main forms (β'$_3$-2L, β'$_2$-2L, β'$_2$-3L and β'$_1$-3L) and a short-life transient β'-2L phase, having d-spacing values very similar to those of β'$_3$-2L (occurring as a splitting of SR-SAXD peaks). The crystallization also consisted of the development of initial β'$_3$-2L, but at significantly higher temperatures than in previously described samples, that is 5 °C and 14 °C above EVOO and the liquid fraction, respectively (Tables 2 and 3). By contrast, β'$_2$-2L form (corresponding to OOO and OOL) crystallized at slightly higher temperatures (just 3 °C difference). One may take into account the considerable decrease in intensity of its corresponding DSC crystallization signal and SR-SAXD peak at 4.4 nm compared to EVOO and the liquid fraction (Figs. 1-4). At an intermediate temperature between crystallization processes of β'$_3$-2L and β'$_2$-2L, the transient phase β'-2L (ts) appeared and transformed to more stable β'$_2$-3L and β'$_1$-3L during successive heating. Most stable β'$_1$-3L form, which did not occur in EVOO or the liquid fraction, was the responsible for the increase in melting temperature (about 4 °C and 15 °C compared to EVOO and the liquid fraction, respectively).

Differences detected in the Solid 4 °C fraction compared to EVOO and the Liquid 4 °C fraction became even more evident for the fraction which still remained in the solid state at 12 °C. Four different polymorphic forms (α-2L, β'$_3$-2L, β'$_2$-3L and β'$_2$-2L) were crystallized from the melt. Additionally and similarly to the Solid 4 °C fraction, transient phase β'-2L(ts) was also detected during cooling, but it just crystallized at the low temperature of about −38 °C, and it simply melted at around −26 °C when heated. However, very few quantities may have been formed, as its characteristic splitting from β'$_3$-2L SR-SAXD peaks were not so evident and, therefore, this form was not detailed or commented in the text and figures. The onset crystallization temperature was set at −3.3 °C, that is 3 °C, 8 °C and 11 °C higher than those of the Solid 4 °C fraction, EVOO and the liquid fraction, respectively. This significant temperature rise was in part due to the occurrence of the initially crystallizing α-2L form, which was not detected in other samples, and the d-spacing values of which coincide with those of α-2L form of the disaturated TAG PPO (Mizobe, Tanaka, Hatakeyama, Nagai, Ichioka, Hondoh, Ueno, & Sato, 2013). Furthermore, DSC and SR-SAXD peaks assigned to the trisaturated OOO and OOL were even more reduced than in the Solid 4 °C fraction. This becomes an indicative of how concentrations of more saturated TAGs increased at the expense of the triunsaturated ones as the melting temperature of fractions was higher, as we will discuss further on, and how can this be explained in terms of polymorphism. Complex polymorphic transformation and multiple melting processes were observed when the Solid 12 °C fraction was heated after crystallization ceased. Most remarkable event was the formation of most stable β'$_1$-3L and β'$_1$-2L polymorphs through phase transition from β'$_2$-3L and β'$_2$-2L, respectively. Thus, melting temperature substantially increased with respect to other samples (reaching a peak top temperature of 16.4 °C and end temperature of 18.1 °C), to which the development of newly formed most stable β'$_1$-2L polymorph may have also greatly contributed.

In Fig. 7, the cooling and heating DSC curves of the raw oil (EVOO), the liquid fraction (Liquid 4 °C fraction), and the solid fraction with highest melting temperature (Solid 12 °C fraction) are compared, demonstrating again the large difference in crystallization and melting temperatures between liquid and solid fractions. As previously detailed, more than 12 °C difference was determined in the crystallization T_{onset} of solid and liquid fractions, and about 18–19 °C variation was determined in corresponding melting T_{top} and T_{end}. Moreover, the intensity of crystallization (~-38 °C) and melting (~-3 °C in the liquid fraction, and ~ 8 °C in EVOO) DSC events associated with β'$_2$-2L form of triunsaturated OOO and OOL increased in the liquid fraction with respect to the EVOO sample, but was significantly diminished (and increased in temperature) in the solid fraction. The significant variations in crystallization and melting temperatures between fractions were also caused by

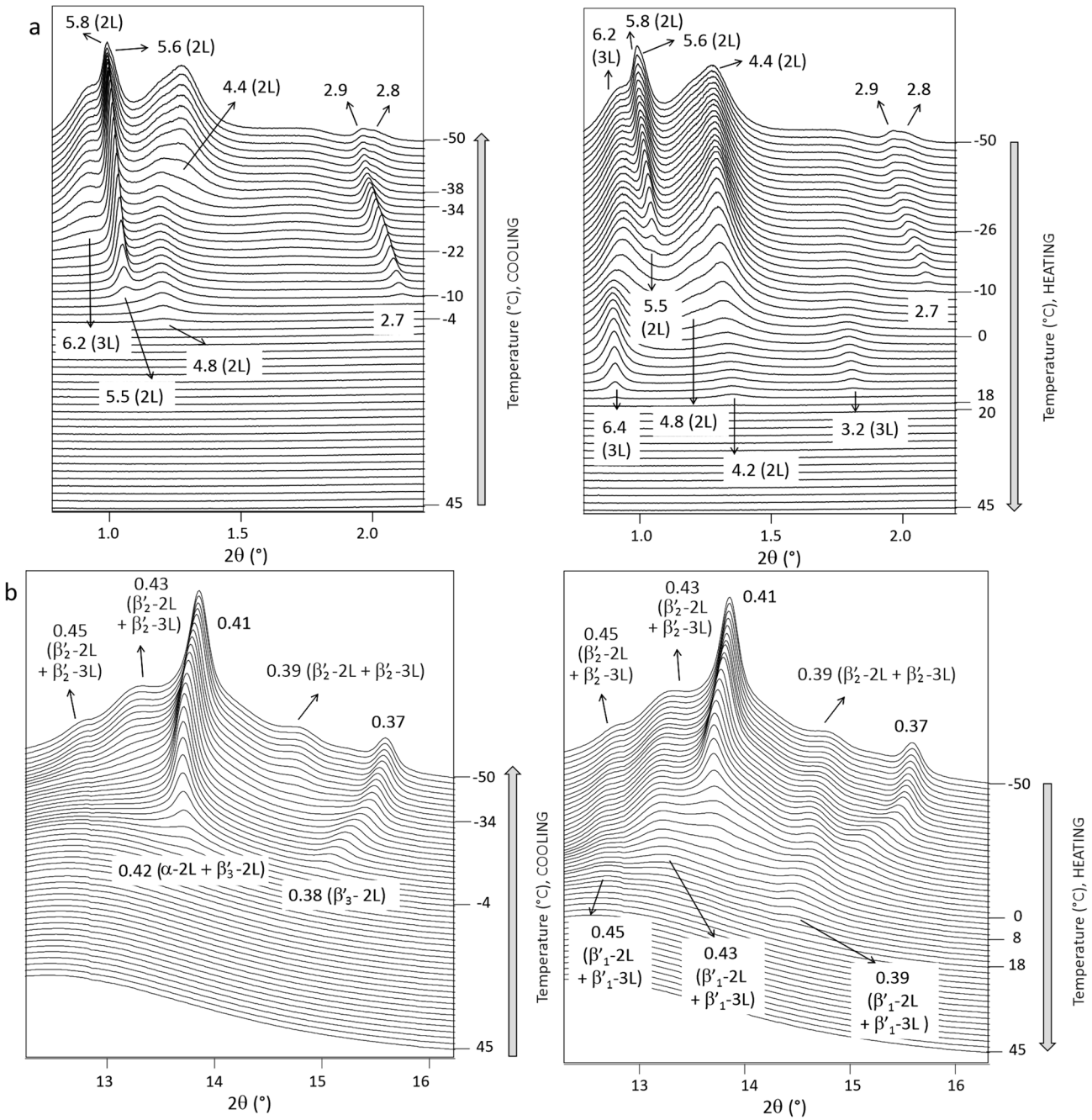

Fig. 5. SR-XRD results of the Solid 12 °C fraction taken under cooling and subsequently heating both at a rate of 2 °C/min. (a) SR-SAXD and, (b) SR-WAXD patterns. Unit: nm.

the occurrence of specific polymorphic forms: just β'$_3$-2L and β'$_2$-2L polymorphs were formed in the liquid fraction, whereas the solid one exhibited additional phases, of which α-2L (PPO) increased the crystallization point, and β'$_1$-3L and β'$_1$-2L raised the melting temperature.

3.2. Fatty acid and tocopherol contents in EVOO and associated fractions

The crystallization and polymorphic behavior of the samples under study were closely related to the saturated–unsaturated nature of component TAGs. To clarify this, Table 4 shows their corresponding fatty acid compositions. Most evident variations were discerned in saturated palmitic acid (C16:0), and unsaturated oleic (C18:1) and linoleic (C18:2) acids. As expected and in view of the relevant differences in the crystallization and polymorphic conduct of the samples, concentrations of most abundant saturated palmitic acid were lower in EVOO (12.9 %) and the liquid fraction (7.7 %) than in solid fractions, and meaningful differences were found between the Solid 4 °C (22.1 %) and the Solid 12 °C fraction (26.8 %). Concerning unsaturated oleic and linoleic acids, their amounts increased in the order Solid 12 °C fraction → Solid 4 °C fraction → EVOO → Liquid 4 °C. Thus, the liquid fraction presented higher amounts of both fatty acids (76.7 % of C18:1 and 9.7 % of C18:2) than EVOO (72.5 % C18:1; 9.0 % C18:2), and concentrations in the last were higher than in the Solid 4 °C fraction (65.0 % C18:1; 6.8 % C18:2) and the Solid 12 °C fraction (61.4 % C18.1; 5.5 % C18:2).

Being the three main fatty acids in EVOO of 100 % Arbequina variety, they are distributed in TAG structures forming triunsaturated OOO as main TAG (about 32–38 %) and OOL (17 %), saturated–unsaturated-unsaturated POO (23–24 %), POL (9–11 %) and SOO (3 %), and

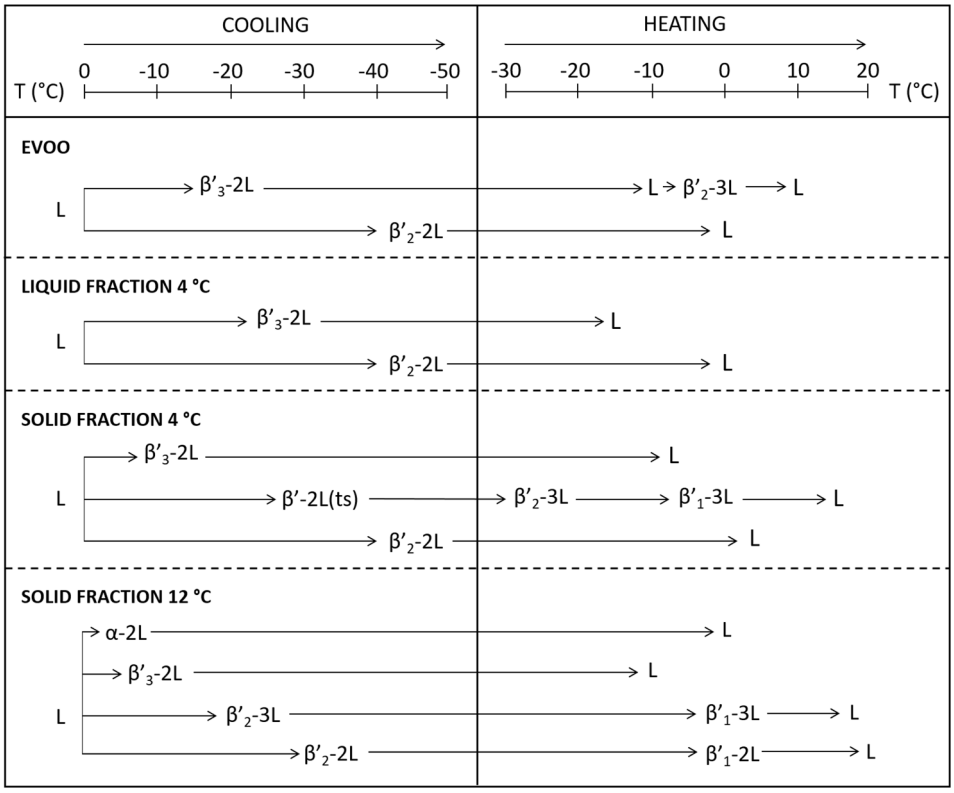

Fig. 6. Summary of polymolymorphic crystallization and transformation pathways of EVOO, and Liquid 4 °C, Solid 4 °C and Solid 12 °C fractions.

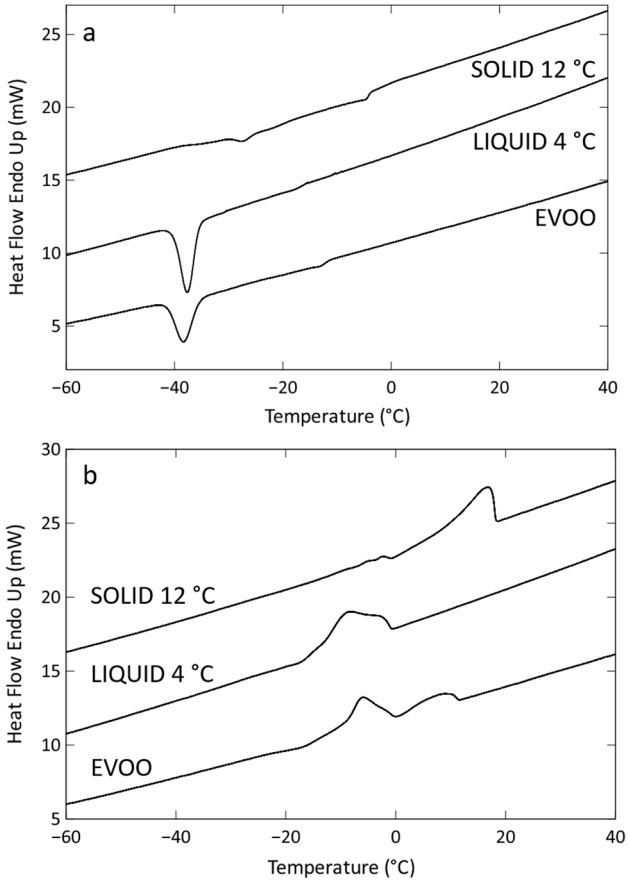

Fig. 7. DSC (a) cooling and (b) heating curves of EVOO, and Liquid 4 °C and Solid 12 °C fractions when cooled and heated at 2 °C/min.

Table 4
Fatty acid compositions (%) of EVOO sample and associated fractions.

	C16:0	C16:1	C18:0	C18:1	C18:2	C18:3	C20:0
EVOO	12.9	1.0	2.0	72.5	9.0	0.7	0.6
Liquid Fraction 4 °C	7.7	1.1	2.1	76.7	9.7	0.8	0.6
Solid Fraction 4 °C	22.1	1.1	2.1	65.0	6.8	0.8	0.8
Solid Fraction 12 °C	26.8	1.0	2.0	61.4	5.5	0.7	0.7

Table 5
α-tocopherol content (mg/kg) in EVOO sample and associated fractions.

	α-tocopherol
EVOO	165
Liquid Fraction 4 °C	150
Solid Fraction 4 °C	66
Solid Fraction 12 °C	47

saturated-saturated–unsaturated PPO (3–5 %) (Jiménez Márquez, & Beltrán Maza, 2003; Jiménez Márquez, Belatrán Maza, Aguilera Herrera, & Uceda Ojeda, 2007). As confirmed by previous work, these main TAG components largely determine the polymorphic behavior of EVOO (Bayés-García, Calvet, Cuevas-Diarte, & Ueno, 2017) and the systematic study of individual TAGs and their mixtures (Bayés-García, Calvet, Cuevas-Diarte, Ueno, & Sato, 2013; Bayés-García, Calvet, Cuevas-Diarte, & Ueno, 2016) allowed us to understand these complex edible oil and also their associated fractions, which were developed in the present work.

Another important issue to consider when evaluating properties and possibilities of EVOO fractions is the determination of tocopherols distribution. α-tocopherol becomes one of the main sources of natural

antioxidant activity in EVOO and, together with phenolic compounds, extensively contributes to its resistance to storage, its stability against oxidation, and makes it more suitable for cooking than other oils (Pellegrini, Visioli, Buratti, & Brighenti, 2001; Fedeli, 1988). As shown in Table 5, the associated liquid fraction obtained retained importantly more α-tocopherol than the solid ones, being the triple amount compared to the Solid 12 °C fraction. However, despite the low concentration of α-tocopherol in solid fractions compared to the liquid one, one may note that they are not negligible and they may play also some part for thermal and storage stability.

The two main fractions obtained from EVOO in this study, having very different crystallization, melting and compositional properties, may be considered for application purposes. The liquid fraction may be of interest due to its high nutritional value owing to the high contents in oleic and linoleic acids, but also in antioxidants such as α-tocopherol. However, special attention may be paid to the Solid 12 °C fraction, the fatty acid composition of which, although being more saturated than that of the native EVOO, is still dictated by a major oleic acid (more than 60 % of total fatty acids). Then, having a mixed saturated/unsaturated composition (with main TAGs POO, POL, SOO and PPO), its crystallization and meting properties (T_m about 16 °C, which is similar to that of the mid fraction of palm oil (Kellens, Gibon, Hendrix, & De Greyt, 2007) may make it suitable for multiple applications as a soft fat. Then, the development of semi-solid textures may imply a step forward in the formulation of trans fatty acids alternatives and the reduction of saturated fats.

4. Conclusions

Fractions of monovarietal EVOO (100 % Arbequina) were obtained by a multi-step dry fractionation method. The three isolated fractions (Liquid 4 °C, Solid 4 °C and Solid 12 °C) exhibited important differences in the crystallization and melting temperatures, and variations were explained through the polymorphic behavior monitored by SR-XRD techniques. Specifically, more than 12 °C and almost 20 °C differences were determined in the crystallization and melting temperatures, respectively, of liquid and solid fractions. These variations were caused by the presence/absence of specific polymorphic forms, owing to different fatty acid compositions forming TAG structures. The potential of EVOO fractions for application in food products among others may be extensively explored. In this sense, it is worth noting the high nutritional value of the liquid fraction (having a T_m of about −3 °C), due to high contents in monounsaturated fats and antioxidants, such as α-tocopherol, and the possibilities of the solid fraction (T_m around 17 °C) to be used as a high-oleic soft fat.

Authors contributions

Laura Bayés-García: Experimental design; experimental procedure execution; data interpretation; manuscript preparation; funding acquisition.

Teresa Calvet: Experimental design; manuscript revision; funding acquisition.

Declarations of interest: None.

Declaration of Competing Interest

The authors declare that they have no known competing financial interests or personal relationships that could have appeared to influence the work reported in this paper.

Acknowledgements

The authors acknowledge the financial support of the Ministerio de Ciencia e Innovación through Project PID2019-107032RB-I00. Funding from the ALBA synchrotron facility is gratefully acknowledged. SR-XRD experiments were performed with the approval of the ALBA Scientific Advisory Committee (proposal 2020074400). The authors thank Dr. Marc Malfois, responsible for the BL11-NCD-SWEET at ALBA, for his assistance.

References

Bayés-García, L., Calvet, T., Cuevas-Diarte, M. A., Ueno, S., & Sato, K. (2013). Crystallization and Transformation of Polymorphic Forms of Trioleoyl Glycerol and 1,2-Dioleoyl-3-rac-linoleoyl Glycerol. *Journal of Physical Chemistry B, 117*, 9170–9181.

Bayés-García, L., Tres, A., Vichi, S., Calvet, T., Cuevas-Diarte, M. A., Codony, R., … Guardiola, F. (2016). Authentication of Iberian dry-cured ham: New approaches by polymorphic fingerprint and ultrahigh resolution mass spectrometry. *Food Control, 60*, 370–377.

Bayés-García, L., Calvet, T., Cuevas-Diarte, M. A., & Ueno, S. (2016). In situ crystallization and transformation kinetics of polymorphic forms of saturated-unsaturated-unsaturated triacylglycerols: 1-palmitoyl-2,3-dioleoyl glycerol, 1-stearoyl-2,3-dioleoyl glycerol, and 1-palmitoyl-2-oleoyl-3-linoleoyl glycerol. *Food Research International, 85*, 244–258.

Bayés-García, L., Calvet, T., Cuevas-Diarte, M. A., & Ueno, S. (2017). From Trioleoyl glycerol to extra virgin olive oil through multicomponent triacylglycerol mixtures: Crystallization and polymorphic transformation examined with differential scanning calorimetry and X ray diffraction techniques. *Food Research International, 99*, 476–484.

Bayés-García, L., Colomer-Llombart, E., Aguilar-Jiménez, M., & Calvet, T. (2021). Polymorphic fingerprint as an approach to authenticate Iberian pig categories. *Journal of the American Oil Chemists' Society, 98*, 1093–1105.

Bootello, M. A., Garcés, R., Martínez-Force, E., & Salas, J. J. (2011). Dry fractionation and crystallization kinetics of high-oleic high-stearic sunflower oil. *Journal of the American Oil Chemists' Society, 88*, 1511–1519.

Chaleepa, K., Szepes, A., & Ulrich, J. (2010). Dry fractionation of coconut oil by melt crystallization. *Chemical Engineering Research and Design, 88*, 1217–1222.

Chiavaro, E., Vittadini, E., Rodriguez-Estrada, M. T., Cerretani, L., Capelli, L., & Bendini, A. (2009). Differential scanning calorimetry detection of high oleic sunflower oil as an adulterant in extra-virgin olive oil. *Journal of Food Lipids, 16*, 227–244.

Cicerale, S., Lucas, L., & Keast, R. (2012). Antimicrobial, antioxidant and anti-inflammatory phenolic activities in extra virgin olive oil. *Current Opinion in Biotechnology, 23*, 129–135.

Damiani, P., Cossignani, L., Simonetti, M. S., Campisi, B., Favretto, L., & Gabrielli Favretto, L. (1997). Stereospecific analysis of the triacylglycerol fraction and linear discriminant analysis in a climatic differentiation of Umbrian extra-virgin olive oils. *Journal of Chromatography A, 758*, 109–116.

Fedeli, E. (1988). The behaviour of olive oil during cooking and frying. In G. Varela, A. E. Bender, & I. D. Morton (Eds.), *Frying of Food, Principles, Changes, New Approaches* (pp. 52–81). Chichester, England, VCH: Ellis Horwood Press.

Ferrari, C., Angiuli, M., Tombari, E., Righetti, M. C., Matteoli, E., & Salvetti, G. (2007). Promoting calorimetry for olive oil authentication. *Thermochimica Acta, 459*, 58–63.

Gutierrez, F., Arnaud, T., & Garrido, A. (2001). Contribution of polyphenols to oxidative stability of virgin olive oil. *Journal of the Science of Food and Agriculture, 81*, 1463–1470.

Harwood, J. L., & Yaqoob, P. (2002). Nutritional and health aspects of olive oil. *European Journal of Lipid Science and Technology, 104*, 685–697.

Jansen, M., & Birch, J. (2009). Composition and stability of olive oil following partial crystallization. *Food Research International, 42*, 826–831.

Jiménez Márquez, A., & Beltrán Maza, G. (2003). Aplicación de la Calorimetría Diferencial de Barrido (CDB) en la caracterización del aceite de oliva virgen. *Grasas y Aceites, 54*, 403–409.

Jiménez Márquez, A., Beltrán Maza, G., Aguilera Herrera, M. P., & Uceda Ojeda, M. (2007). Calorimetría diferencial de barrido. Influencia de la composición del aceite de oliva virgen en su perfil térmico. *Grasas y Aceites, 58*, 122–129.

Kellens, M., Gibon, V., Hendrix, M., & De Greyt, W. (2007). Palm oil fractionation. *European Journal of Lipid Science and Technology, 109*, 336–349.

Larsson, K., Quinn, P., Sato, K., & Tiberg, F. (Eds.). (2006). *Lipids: Structure, physical properties and functionality*. Bridgewater: The Oily Press.

Maggio, R. M., Barnaba, C., Cerretani, L., Paciulli, M., & Chiavaro, E. (2014). Study of the influence of triacylglycerol composition on DSC cooling curves of extra virgin olive oil by chemometric data processing. *Journal of Thermal Analysis and Calorimetry, 115*, 2037–2044.

Mizobe, H., Tanaka, T., Hatakeyama, N., Nagai, T., Ichioka, K., Hondoh, H., … Sato, K. (2013). Structures and Binary Mixing Characteristics of Enantiomers of 1-Oleoyl-2,3-dipalmitoyl-*sn*-glycerol (S-OPP) and 1,2-Dipalmitoyl-3-oleoyl-*sn*-glycerol (R-PPO). *Journal of the American Oil Chemists' Society, 90*, 1809–1817.

Pellegrini, N., Visioli, F., Buratti, S., & Brighenti, F. (2001). Direct Analysis of Total Antioxidant Activity of Olive Oil and Studies on the Influence of Heating. *Journal of Agricultural and Food Chemistry, 49*, 2532–2538.

Timms, R. E. (2005). Fractional crystallization - The fat modification process for the 21st century. *European Journal of Lipid Science and Technology, 107*, 48–57.

Vichi, S., Pizzale, L., & Conte, L. S. (2007). Stereospecific distribution of fatty acids in triacylglycerols of olive oils. *European Journal of Lipid Science and Technology, 109*, 72–78.

Vlahov, G., & Angelo, C. S. (1996). The Structure of Triglycerides of Monovarietal Olive Oils: A ^{13}C-NMR Comparative Study. *Fett/Lipid, 98*(6), 203–205.

Wagner, K. H., & Elmadfa, I. (2000). Effects of tocopherols and their mixtures on the oxidative stability of olive oil and linseed oil under heating. *European Journal of Lipid Science and Technology, 102*, 624–629.

Zaliha, O., Chong, C. L., Cheow, C. S., Norizzah, A. R., & Kellens, M. J. (2004). Crystallization properties of palm oil by dry fractionation. *Food Chemistry, 86*, 245–250.